npj | climate and atmospheric science

Article

Published in partnership with CECCR at King Abdulaziz University

https://doi.org/10.1038/s41612-026-01398-5

Confirming the substantial contribution of ozone-depleting halocarbon emissions to global warming during the second half of the 20th century

Check for updates

M. Friedel[1,14] ✉, G. Chiodo[2,3,14] ✉, K. Weber[3,14] ✉, L. M. Polvani[4,5], J. S. Daniel[6], N. L. Abraham[7,8], S. M. Davis[6], M. Deushi[9], N. Oshima[9], L. W. Horowitz[10], J. F. Lamarque[11], J. Keeble[12], L. Nazarenko[13] & C. Orbe[13]

Ozone-depleting halocarbons (OD-HCs) are potent greenhouse gases but can also cause radiative cooling by depleting stratospheric ozone. Previously, global climate models revealed substantial OD-HC-driven warming in the second half of the 20th century, with only partial offset by ozone loss. More recent estimates of OD-HC net effective radiative forcing (ERF), however, have raised the possibility of much larger cancellation from ozone depletion, questioning the climatic co-benefits of the Montreal Protocol, which led to the worldwide phase-out of OD-HCs. Here, analyzing several comprehensive chemistry-climate models with realistic stratospheric ozone depletion, we confirm that the OD-HC net ERF is extremely likely positive, with a best estimate of ~ 0.2 W m^{-2} for 2014, consistent with earlier estimates showing only a partial offset by ozone depletion. Furthermore, our results demonstrate that, had OD-HC emissions not occurred in the second half of the 20th century, global warming during that period would have been around 20% lower, confirming the critical co-benefit of the Montreal Protocol in mitigating global warming.

Ozone-depleting halocarbons (OD-HCs) were the major driver of stratospheric ozone depletion during the second half of the 20th century[1]. Following the adoption of the Montreal Protocol in 1987, their emissions were largely phased out, leading to a gradual decline in their overall atmospheric abundances since the early 21st century[2]. This phase-out prompted the transition to hydrofluorocarbons (HFCs) as ozone-safe replacement compounds. In addition to depleting ozone, OD-HCs–as well as their replacement gases–are potent greenhouse gases, with global warming potentials (GWP) that can be thousands of times higher than that of CO_2 (e.g., for GWP_{100}) for some OD-HCs[3–5]. Thus, reductions in OD-HC emissions may have played an important role in mitigating past and future global warming, in addition to protecting the ozone layer[6]. However, the net impact of OD-HCs on past global warming–and the extent to which the Montreal Protocol can be considered a climate treaty–remains debated[7,8].

Quantifying the climate impact of OD-HCs is complicated by competing radiative effects. While OD-HCs exert a positive effective radiative forcing (ERF), the associated depletion of stratospheric ozone induces a negative ERF that partially offsets this warming. The net forcing, therefore, depends on the magnitude of ozone-related cooling and other atmospheric adjustments, such as changes in clouds and atmospheric composition[9–11].

The degree to which ozone depletion offsets the OD-HC ERF–and thus the net climate forcing of OD-HCs–has been a subject of considerable debate since the 1990s[12,13], and recent assessments illustrate that the net radiative and climatic impacts of OD-HCs still remain uncertain. For the year 2019 (relative to pre-industrial conditions), IPCC AR6 Chapter 7 estimates a direct ERF of OD-HCs of 0.354 W m^{-2} (uncertainty of around 20%) based on atmospheric concentrations and radiative efficiencies[11]. Emission-based estimates from the Aerosol Chemistry Model

[1]Institute for Meteorology, University of Leipzig, Leipzig, Germany. [2]Instituto de Geociencias, Spanish National Research Council (IGEO-CSIC), Madrid, Spain. [3]Institute for Atmospheric and Climate Science, ETH Zurich, Switzerland. [4]Department of Applied Physics and Applied Mathematics, Columbia University, New York, NY, USA. [5]Lamont Doherty Earth Observatory, Columbia University, Palisades, NY, USA. [6]NOAA Chemical Sciences Laboratory, Boulder, CO, USA. [7]Yusuf Hamied Department of Chemistry, University of Cambridge, Cambridge, UK. [8]National Centre for Atmospheric Science, West Yorkshire, UK. [9]Meteorological Research Institute, Tsukuba, Japan. [10]NOAA Geophysical Fluid Dynamics Laboratory, Princeton, NJ, USA. [11]National Center for Atmospheric Research. Now at Climate Modeling and Analysis, LLC, Superior, CO, USA. [12]Lancaster Environment Centre, Lancaster University, Lancaster, UK. [13]NASA Goddard Institute for Space Studies, New York, NY, USA. [14]These authors contributed equally: M. Friedel, G. Chiodo, K. Weber. ✉e-mail: marina.friedel@uni-leipzig.de; gabriel.chiodo@csic.es; konstantin.weber@env.ethz.ch

Intercomparison Project (AerChemMIP,[14]) reported in IPCC AR6 Chapter 6[9,10] are somewhat higher, around ~ 0.41 W m^{-2}.

In turn, the IPCC AR6 provides estimates of the OD-HC-induced ozone ERF, but inconsistencies exist between its chapters. Chapter 7[11] estimates an OD-HC-induced ozone ERF of − 0.11 ± 0.10 W m^{-2} based on AerChemMIP results[9] (after excluding the UKESM model due to excessive ozone depletion). Chapter 6[10], by contrast, reports a larger cancellation due to ozone depletion of − 0.162 W m^{-2}. As a result, AR6 Chapter 6 derives a best estimate of the net (also called total) ERF from OD-HCs of approximately 0.17 W m^{-2} for 2019, with a very likely range that extends toward near-zero values. Chapter 6 further acknowledges that AR6 models may have biases in their simulation of stratospheric ozone, affecting their estimates of radiative impacts of OD-HCs. This slight internal inconsistency in IPCC AR6 illustrates that the net climate effect of OD-HCs remains uncertain.

Another reason why the latest IPCC did not arrive at a robust conclusion regarding the radiative impacts of OD-HCs were the results of two studies that applied observational constraints on historical ozone trends from AerChemMIP simulations. The first study estimated that the ERF from OD-HCs is close to zero when accounting for the accompanying ozone depletion, with a best estimate of 0.04 W m^{-2} and an uncertainty spanning over negative values (− 0.05 to 0.13 W m^{-2})[7]. Methodological refinements in a subsequent analysis yielded a slightly higher ERF of 0.085 ± 0.059 W m^{-2}[8]. While likely positive (84%), this latter estimate is about 50% smaller than estimates from the IPCC (~ 0.17 W m^{-2})[10], and therefore implies a much smaller climate co-benefit of the Montreal Protocol than previously thought[7,8].

These constrained net ERF estimates for OD-HCs, however, should be treated with caution. In addition to the potential impact of internal variability–due to the short time period considered and small available ensemble sizes–the observational constraint used in these studies was based on *total column ozone*[7,8]. This approach, however, conflates stratospheric ozone depletion due to OD-HCs with tropospheric ozone increases driven predominantly by emissions of ozone precursors that are largely independent of OD-HC emissions.

Despite these limitations, the small net OD-HC ERF reported by ref. 8 served as the basis for a recent study of the indirect forcing effects of ozone depletion on the net OD-HC ERF[15]. This study concludes that ozone-depletion-induced changes in methane (CH_4) lifetime could contribute as much as − 0.06 W m^{-2}, potentially further reducing the net ERF of OD-HCs to nearly zero. However, since these results rely on the ozone ERF estimates from ref. 8, their robustness hinges on the assumption that observational constraints on total column ozone are physically justifiable. Moreover, the multi-model mean values presented by ref. 15 may be disproportionately influenced by individual models with biases in ozone depletion trends.

Although ERF quantifies the radiative perturbation from OD-HCs, the magnitude of the resulting warming depends critically on climate feedbacks that the ERF does not capture[16]. The net ERF of OD-HCs and HFCs in IPCC AR6 Chapter 6 corresponds to a positive contribution to historical global warming of approximately 0.102 °C (0.005–0.210 °C), calculated with an idealized two-layer climate emulator[10]. Of this, approximately 0.04 W m^{-2}, corresponding to 0.019 °C, is attributable to HFCs, implying a total OD-HC-induced warming of ~ 0.08 °C. Two other studies confirmed this OD-HC-induced surface warming in comprehensive climate models, using large ensembles, and thereby separating the forced response from internal variability. The first study found that global warming would have been approximately 30% smaller (and Arctic warming 50% smaller) than observed without emissions of ozone-depleting substances (ODS, comprising OD-HCs) in the second half of the 20th century[17]. These findings were corroborated by a second study, which employed an even larger ensemble of simulations from a different climate model, and found that ODS accounted for 30% of anthropogenic global warming between 1955 and 2005[18]. The latter study did not include interactive atmospheric chemistry, but imposed an ozone field compiled for CMIP6[19], which exhibits realistic stratospheric depletion trends. If the net OD-HC ERF was indeed near zero, as suggested by refs. 7,15, this forcing would be physically difficult to reconcile with the substantial 30% warming contribution identified in large-ensemble simulations.

To reduce the remaining uncertainty of the OD-HC net ERF and its contribution to past global warming, we leverage a suite of comprehensive chemistry-climate model simulations. Crucially, we incorporate a range of additional simulations and introduce new observational constraints based solely on stratospheric ozone changes, thereby avoiding confounding effects from historical tropospheric ozone changes. Our approach provides a systematic methodology to constrain uncertainties in OD-HC ERF and the resulting temperature response using model-weighting based on observational constraints.

Results

Attribution of stratospheric temperature and ozone changes to OD-HCs

We begin by examining historical ozone changes in the six comprehensive chemistry-climate models from CMIP6[20], which interactively simulate atmospheric composition and climate changes under historical emissions (see Methods). We use simulations from AerChemMIP[14], supplemented with additional ensemble members, and compare decadal mean differences between 1955–1964 and 1996–2005. We further include available CESM1-WACCM simulation data from ref. 17 in our analysis. As shown in Fig. 1, all models show a decrease in stratospheric ozone, especially over the polar regions, while tropospheric ozone has increased, particularly in the Northern Hemisphere. However, the models differ substantially in the magnitude (and pattern) of these changes, with UKESM1-0-LL and MRI-ESM2-0 representing the two extremes. Notably, UKESM1-0-LL, a known outlier for ozone depletion[21,22], simulates an unrealistically large ozone decline throughout the lower stratosphere, whereas decreases in MRI-ESM2-0 are modest and mostly confined to the Antarctic stratosphere. These inter-model differences are consistent with previous assessments[21]. For comparison, the Japanese reanalysis (JRA-3Q)[23,24] indicates stratospheric ozone changes more in line with models that show smaller ozone losses.

Ozone observations before the 1980s are sparse and uncertain, complicating the evaluation of reanalysis products and model performance during this period. Nevertheless, including years before the satellite era improves statistical confidence, since (1) a longer time window allows us to calculate the ozone climatologies over ten rather than five years, which is critical given the large inter-annual variability of stratospheric ozone, and (2) we capture ozone changes that occurred before the 1980s.

To isolate the effects of OD-HCs, we contrast historical runs (Fig. 1) with simulations keeping OD-HC concentrations constant at 1950 levels (*hist-1950HC*). Supplementary Fig. 1 reveals that tropospheric ozone is only slightly affected by OD-HC emissions–especially in the low latitudes–while stratospheric ozone changes can largely be attributed to OD-HC-driven chemical depletion (Fig. 1). This is consistent with the results from ref. 25, who found that halocarbons mainly affect stratospheric ozone, and to a lesser extent, tropospheric ozone. Since ozone depletion reduces shortwave absorption, thereby cooling the stratosphere[26], differences in historical stratospheric ozone loss translate directly into differences in stratospheric temperature changes. Consequently, the extent of stratospheric ozone decline can be closely linked to cooling in the lower stratosphere, given that radiative cooling by CO_2 is comparatively small there[27]. The vertical pattern of historical temperature change (Supplementary Fig. 2) reveals widespread lower stratospheric cooling, between 1955–1964 and 1996–2005 (hereinafter the "historical period"), especially in the polar regions. The pattern of stratospheric temperature changes attributed to OD-HCs (Supplementary Fig. 3) closely mirrors overall ozone changes (Fig. 1), highlighting the dominant role of OD-HC-driven ozone depletion in shaping lower stratospheric temperature trends. Figure 2 further illustrates this, by relating global mean stratospheric partial ozone column changes and

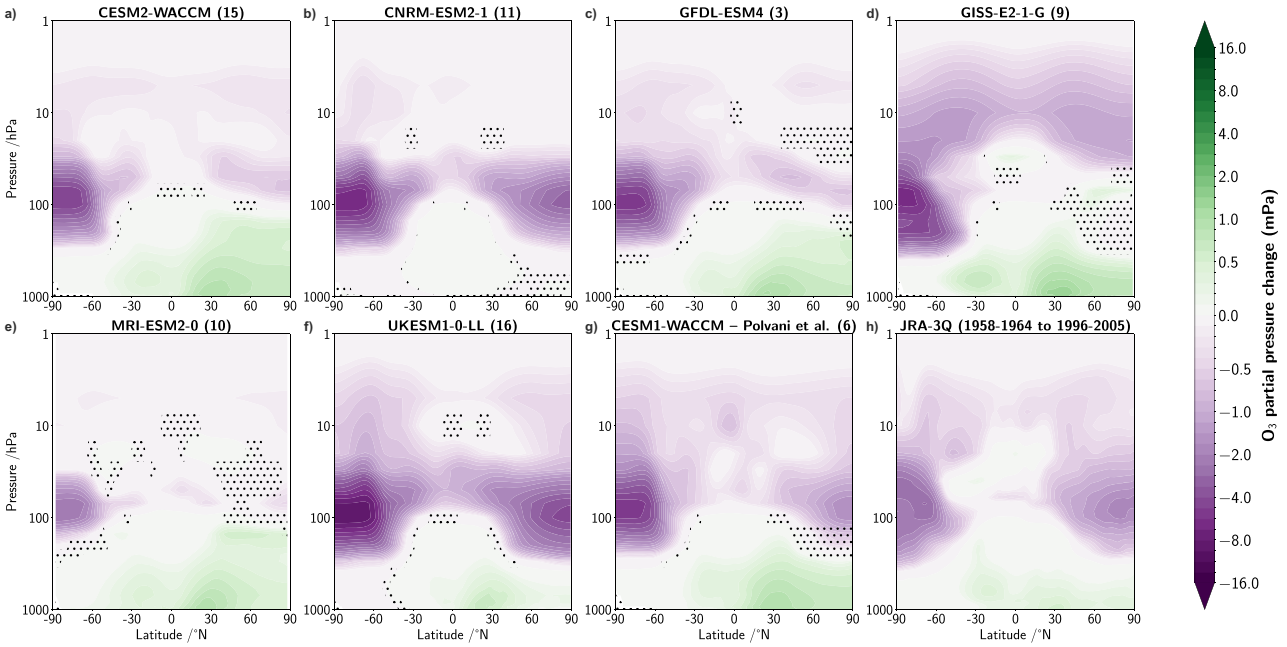

Fig. 1 | Zonal mean ozone changes in the historical period. Zonal mean ozone changes from 1955–1964 to 1996–2005 in the *historical* simulations of AerChemMIP models (**a**–**g**). Units are partial pressure changes, in mPa. Numbers in brackets denote the number of ensemble members available in the *historical* ensemble, respectively. Dots identify changes that are not statistically significant at the 95% level. **h** Shows zonal mean ozone changes in JRA-3Q for comparison. Note the non-linear colorbar. The height of the tropopause depends on the latitude (around 300 hPa at the poles and around 70 hPa in the tropics) and closely follows the ozone depletion pattern in the Southern Hemisphere. The strongest ozone depletion is found in the polar lower stratosphere, mostly between 200 and 30 hPa.

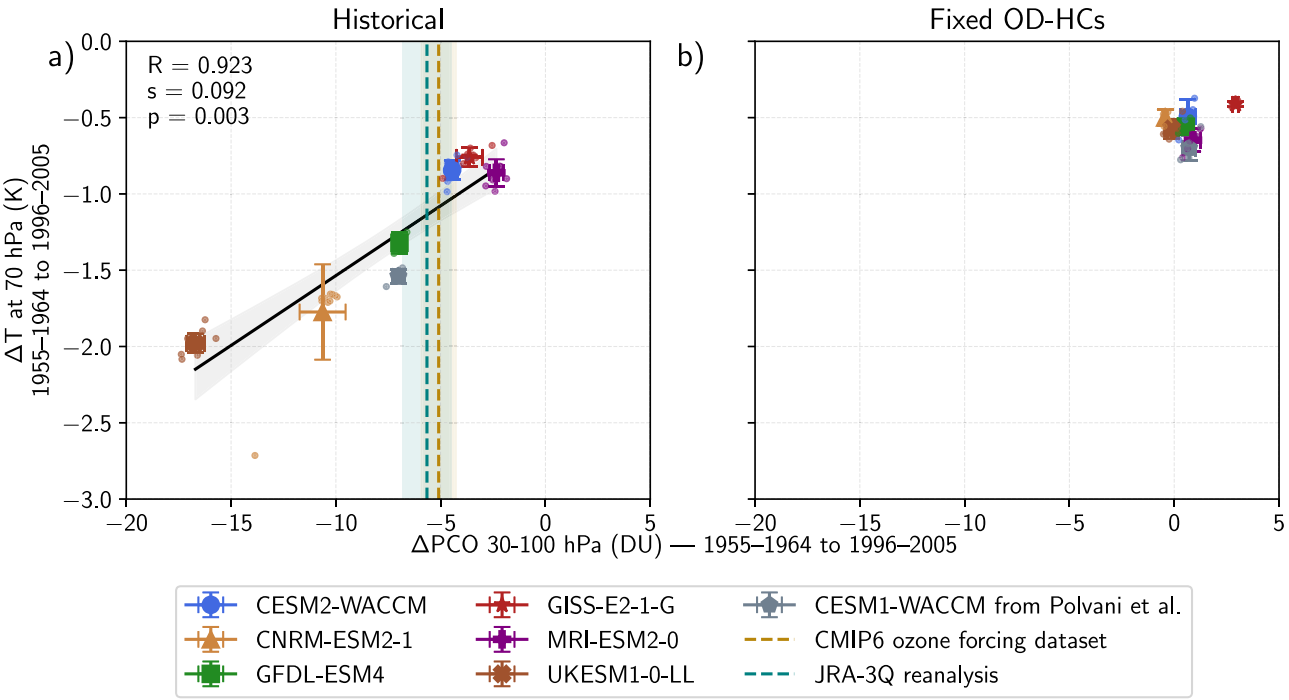

Fig. 2 | Relation between global mean historical stratospheric ozone and temperature changes. Changes in global mean stratospheric PCO vs. temperature changes at 70 hPa for the historical period in *historical* simulations (**a**) and *hist-1950HC* simulations (**b**) for different models. Error bars show the standard deviation across ensemble members. Vertical lines in (**a**) indicate the PCO change in the CMIP6 ozone forcing dataset (brown) and the JRA-3Q reanalysis (green). Shown are also the values for the Pearson correlation coefficient (R), slope (s), and p value of the slope (p) in (**a**).

temperature changes in the lower stratosphere across models for the historical period, consistent with previous studies[28,29]. Simulations with OD-HC concentrations fixed at 1950 levels exhibit minimal stratospheric cooling of − 0.5 °C, as expected from increasing CO_2 emissions (Fig. 2b). Overall, the inter-model spread in lower stratospheric temperature changes is attributable to OD-HC-induced ozone depletion simulated in these models, highlighting the causal link between stratospheric ozone decline and lower stratospheric cooling.

For further validation against more observational datasets, we additionally focus on a period within the satellite era (beginning in the 1980s), using the timeframe between 1985–1989 and 2001–2005 (hereinafter the "satellite period"). During this period, the relationship found in Fig. 2a

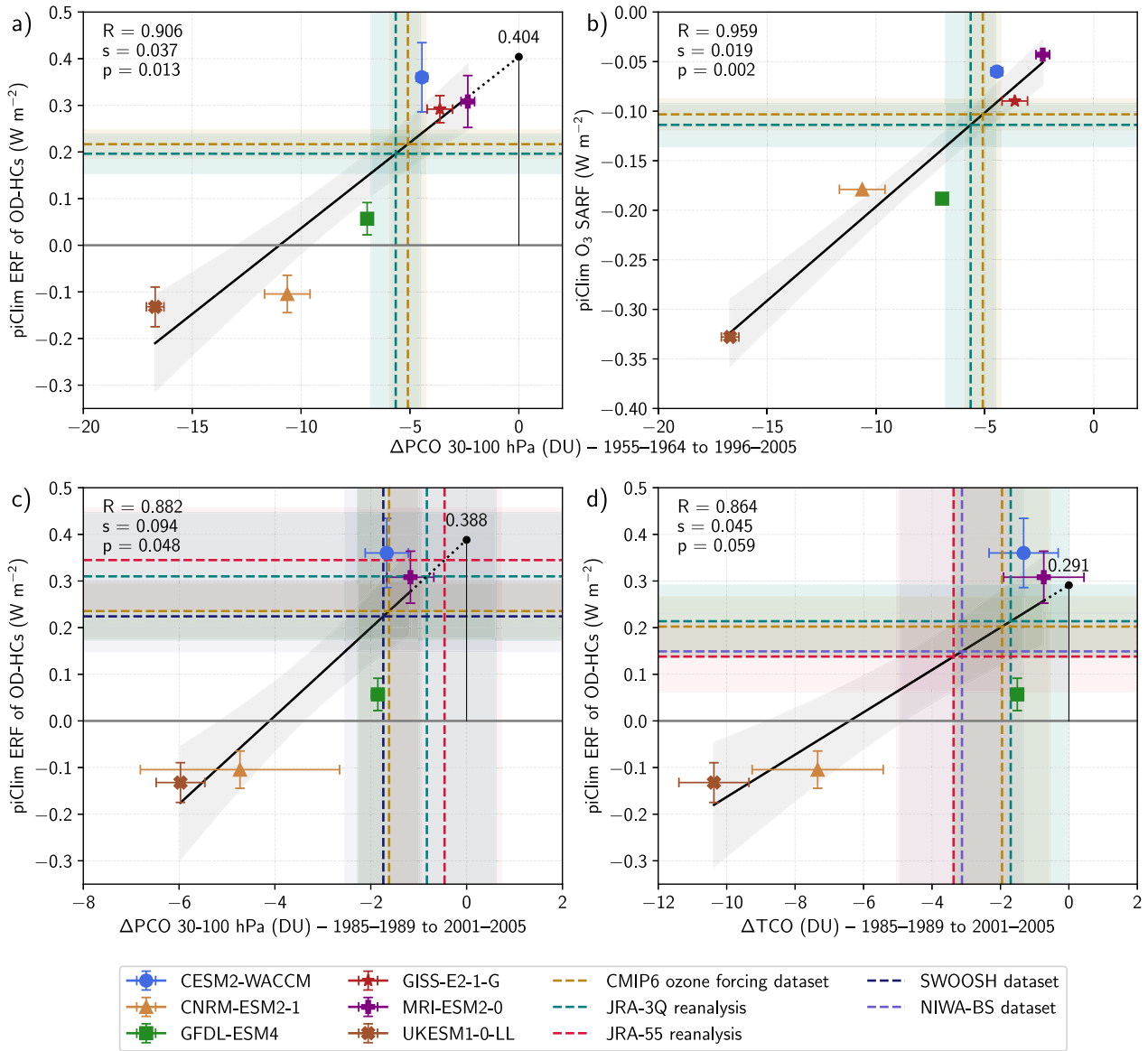

Fig. 3 | Correlation between historical ozone changes and OD-HC-induced Effective Radiative Forcing across models. Relationship between PCO changes in the *historical* simulations and (**a**) the ERF and (**b**) the ozone SARF across models for the historical period. For the satellite period, relationships are shown between (**c**) PCO changes in *historical* simulations and the OD-HC ERF, and (**d**) TCO changes and the OD-HC ERF. The OD-HC ERF for each model is derived from timeslice simulations, while ozone SARF values are taken from ref. 9. Each panel shows the linear regression between ozone changes and the ERF (black line) with its uncertainty (gray shading). Vertical stippled lines mark ozone changes from observational datasets, with shading indicating observational uncertainty due to internal variability. Horizontal stippled lines show the inferred OD-HC ERF for each dataset estimated from the regression. In each panel, the values for the Pearson correlation coefficient (R), slope (s), and p value of the regression slope (p) are shown. Note that GISS-E2-1-G is excluded in the satellite period (panels c and d) due to its bias in the response to volcanic aerosols.

remains consistent with earlier findings (Supplementary Fig. 4), except for the GISS-E2-1-G model. This model shows strong stratospheric cooling and ozone loss even when OD-HCs are held at 1950 levels (see Supplementary Fig. 4), a behavior linked to its very high sensitivity to volcanic eruptions[7]. Accordingly, for the satellite period, we exclude GISS-E2-1-G from our analyses, as in refs. 7,8.

Taken together, these results confirm that simulated ozone depletion due to OD-HCs drives inter-model differences in historical stratospheric temperature changes.

Constraining the OD-HC net ERF using historical ozone changes

Next, we assess how ozone changes across models relate to differences in OD-HC net ERF. In the following, we omit the "net" and refer to this as just the OD-HC ERF. For each model, the OD-HC ERF is derived from dedicated time-slice simulations with fixed sea-surface temperatures (SSTs), by contrasting top-of-atmosphere radiation fluxes in simulations with pre-industrial (*piClim-control*) vs. present-day (year 2014, *piClim-HC*) OD-HC concentrations (see Methods). Figures 3a, c show a strong correlation ($R \approx 0.9$) between stratospheric partial column ozone (PCO) changes and OD-HC ERF for both the historical (panel a) and satellite periods (panel c), suggesting that differences in ozone depletion are an important contributor to inter-model uncertainty in ERF. The regression intercept at zero ozone change corresponds to the OD-HC ERF in the hypothetical absence of ozone depletion. This is similar to the direct concentration-based ERF, as it may still include other atmospheric adjustments such as circulation and cloud changes. For the historical period (panel a), the intercept is 0.404 W m^{-2} (90% confidence interval: 0.341–0.467 W m^{-2})–consistent with the direct ERF estimates of 0.354 and 0.41 W m^{-2} from the IPCC

AR6[11,30]. For the satellite period (panel c), the regression yields a similar value of 0.388 W m^{-2} (0.305–0.464 W m^{-2}).

One might question if this ERF-ozone relationship is driven solely by ozone changes or is also influenced by rapid adjustments, such as cloud variations[31]. To isolate the role of ozone, we repeat the analysis using the stratospherically adjusted radiative forcing (SARF)[32], which reveals an even stronger linear correlation (panel b), indicating that OD-HC-associated ozone depletion is the primary mechanism underlying the ERF-ozone relationship. SARF from ozone offsets part of the direct OD-HC warming effect, and differences in ozone changes across models are the leading cause of the spread in the overall ERF. Tropospheric ozone changes may also partly contribute, as suggested by ref. 25, although their contribution to the ERF might be smaller, given the small changes in tropospheric ozone from OD-HCs in AerChemMIP models (Figs. 1 and S1). Small ozone changes near the tropopause may still disproportionately affect the ERF, though their integrated effect, along with their contribution to ERF and SARF uncertainty across models, is likely to be small. Another aspect worthy of being highlighted is that the regression slope is significantly steeper for the ERF than the SARF, suggesting that other adjustments such as circulation and clouds partly amplify the ozone ERF, though their detailed contribution would need to be assessed with other radiative kernels, which have their methodological caveats (i.e. they are based on a specific model's radiation scheme and cloud climatology).

The wide spread in modeled ozone depletion raises questions about how to handle outliers, which strongly impact the multi-model mean OD-HC ERF, despite lacking physical plausibility. Here, we use observational constraints to leverage the robust, physically-based linear relationship between the models' OD-HC ERF and historical ozone loss, and derive estimates for the OD-HC ERF informed by observed ozone changes.

Using bootstrapping to propagate uncertainties (see Methods), we construct constrained ERF distributions for each observational dataset and period. For the historical period, with only one reliable ozone reanalysis (JRA-3Q), we obtain a constrained ERF of 0.196 W m^{-2} (0.119–0.276 W m^{-2}) for 2014 OD-HC levels; this uncertainty range includes uncertainty in the observed ozone change, and in the slope and intercept of the regression (thus, the models' internal variability). In the shorter satellite period, additional observational datasets are available, which differ in their inferred ozone changes (Fig. 3c): their median constrained OD-HC ERF values range from 0.22 to 0.34 W m^{-2} (distributions are shown in Supplementary Fig. 5). Our best estimate, based on the merged satellite product SWOOSH[33], is 0.222 W m^{-2}, slightly larger than the IPCC AR6 estimate of 0.17 W m^{-2}. In addition, the CMIP6 forcing dataset closely matches the ozone depletion in re-analysis products for both time periods. Despite large differences between observational data sets, the lower bound (5th percentile) of the constrained ERF remains positive (0.08–0.15 W m^{-2}), making any net cooling effect of OD-HC emissions extremely unlikely. Taken together, ozone depletion offsets at most around 50% of the direct OD-HC-induced warming, confirming that historical OD-HC emissions contributed significantly to global warming over the second half of the 20th century (between 1955–1964 and 1996–2005).

To reconcile differences with previous studies using observational constraints based on total column ozone (TCO), we evaluate the linear relationship between TCO changes and OD-HC ERF during the satellite period (Fig. 3d). This relationship is still present, but is weaker than the one based on PCO. Applying observational constraints using TCO changes with data from NIWA-BS yields a smaller constrained OD-HC ERF (0.149 W m^{-2}; 90% confidence interval: 0.009–0.293 W m^{-2}). Across all constraints, the ERF derived from TCO (Fig. 3d) is consistently lower than that from PCO (Fig. 3c). This result is closer to the earlier estimate of 0.085 W m^{-2} reported by ref. 8, but remains around 40% larger and consistently positive. The remaining discrepancy from refs. 7,8 likely reflects the larger number of simulations available in our analysis, which enhances statistical robustness. Additionally, methodological differences in quantifying ozone changes–such as using trends vs. absolute changes–may contribute to these discrepancies. Crucially, the smaller ERF derived using observational constraints on TCO compared to PCO likely arises because TCO includes tropospheric ozone variations driven by precursors unrelated to OD-HC emissions. This suggests that TCO is a less reliable proxy for OD-HC-induced ERF than PCO.

Impact of OD-HCs on historical global temperature changes

Having confirmed that the historical OD-HC ERF (up to 2014) is extremely likely (> 95%) positive, we estimate its contribution to global warming since the mid-20th century. To address this, we analyse the OD-HC-induced global surface temperature changes between 1955–1964 and 1996–2005 by comparing historical simulations with simulations fixing OD-HCs at 1950 levels. The six climate models with available *piClim* simulations exhibit a wide spread in OD-HC-induced surface temperature changes (− 0.2 to + 0.2 °C), with two models (UKESM1-0-LL and CNRM-ESM2-1) even showing a net cooling effect from OD-HCs. Figure 4a reveals a highly significant correlation between the OD-HC-induced ERF and the OD-HC-induced global mean surface temperature changes: Models with higher ERFs show stronger warming, whereas those with small or negative ERFs exhibit cooling from OD-HC emissions.

Building on this relationship, Fig. 4b displays the total surface temperature changes in historical simulations (black bars) and those with fixed OD-HCs (pink bars), now also including CESM1-WACCM simulations from ref. 17. The models exhibit considerable differences in their overall temperature responses under historical forcing, ranging from 0.4 to 0.8 °C. Figure 4c) isolates the effect of OD-HCs on surface temperature by subtracting temperature changes from fixed-HC simulations from full-forcing historical simulations. Models with negative OD-HC ERF (blue) are also the only ones simulating a cooling from OD-HCs, whereas models with positive ERFs (red) exhibit positive temperature changes.

Although surface temperature changes cannot generally be accurately predicted from the ERF alone (due to differences in radiative efficacy and feedbacks), the strong correlation between these variables in Fig. 4a, together with the coherence in the sign of the ERF and temperature changes in Fig. 4b, c, strongly hints that the OD-HC ERF provides some predictive insights into the direction of surface temperature changes.

To quantify the overall surface temperature response of OD-HCs, we calculate weighted multi-model means. Since the ERF is closely linked to PCO changes (see Fig. 3a, c), models that more accurately reproduce observed past ozone changes are expected to have a more realistic ERF and, consequently, more realistic surface temperature responses. Thus, we weight models based on their skill in simulating historical stratospheric ozone changes during both the historical period (JRA-3Q) and the satellite period (SWOOSH). Best estimates for the weighted model means are 0.136 °C (0.055–0.211 °C) based on SWOOSH and 0.112 °C (0.071–0.156 °C) using JRA-3Q (full distributions in Supplementary Fig. 6). These values correspond to around 20% of the overall global mean surface temperature changes from 1960 to 2000. Both weighting approaches yield similar estimates, revealing a robust positive contribution of OD-HC emissions to global warming in that time period, regardless of the observational ozone dataset or period used.

Our best estimates are comparable to the IPCC AR6 value of 0.08 °C[10], despite the IPCC value being based on a much simpler methodology, involving the use of an emulator to convert the ERF into surface temperature changes instead of coupled chemistry-climate models. However, our estimates suggest that the IPCC value might be underestimated by 30%, likely reflecting the role of outliers (such as the UKESM model) on the IPCC multi-model mean estimate. Since the model weighting framework presented here is designed to evaluate and weight models based on observations, we deem our results to be more robust than a simple multi-model mean. Thus, we conclude that OD-HCs have been a significant driver of global warming over the second half of the 20th century (1955–2005). These findings emphasize that historical OD-HC emissions have almost certainly exerted a net warming influence, underscoring the critical co-benefit of the Montreal Protocol in mitigating additional global warming.

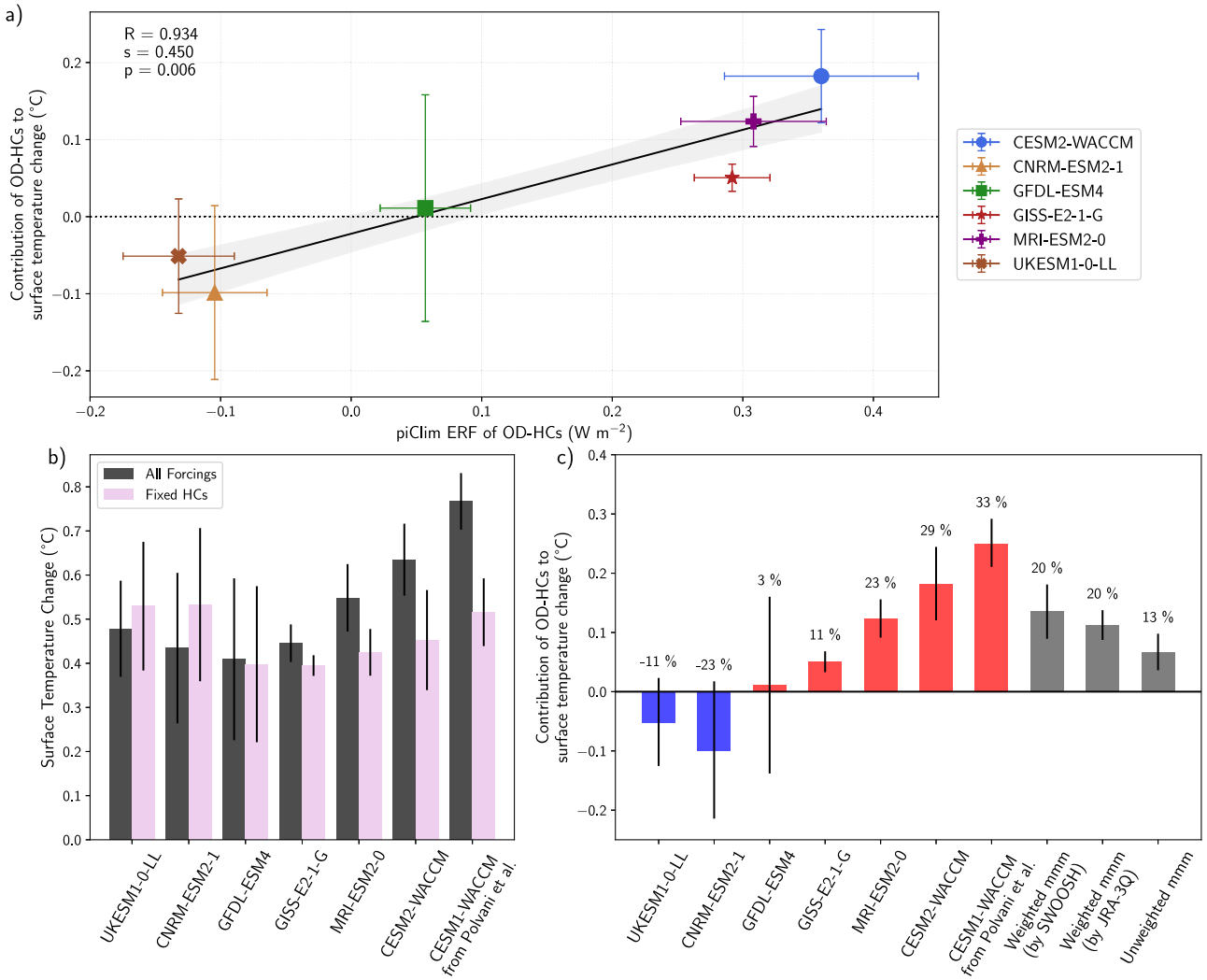

Fig. 4 | Effective Radiative Forcing and global surface temperature changes induced by OD-HC emissions. OD-HC ERF versus OD-HC-induced surface temperature change across models (**a**) modeled warming over the historical period in the ensembles with (All Forcings--black bars) and without (Fixed OD-HCs--violet bars) OD-HC changes in each the models (**b**) and OD-HC-induced surface temperature change (**c**), highlighting the models with a positive OD-HC ERF in red, and a negative OD-HC ERF in blue, including WACCM4 data from ref. 17. Gray bars in (**c**) show the weighted multi-model medians (MMM), with weights being based on the ability of models in reproducing observed ozone changes over the satellite period in SWOOSH data, over the extended period in JRA-3Q data, and the unweighted multi-model median. Percentages in (**c**) denote the derived median relative contribution of OD-HC-induced warming to overall global warming.

Discussion

In summary, our study confirms that OD-HCs contributed around 20% to global warming in the second half of the 20th century (1955–2005)–despite some cooling due to the accompanying ozone depletion. We also identify stratospheric ozone depletion as the leading source of inter-model spread in OD-HC ERF estimates. These results underscore the climatic co-benefit of the Montreal Protocol: without it, uncontrolled OD-HC emissions would have produced far greater warming, as the cooling from ozone depletion only partially offsets their direct radiative forcing[6,34–38].

We note that our ERF estimates may not fully capture the additional negative forcing from OD-HC-induced reductions in CH_4 lifetime.[15] suggests that, over the recent past (1950–2014), such indirect forcings from ozone and CH_4 lifetime changes lead to strong cancellation of OD-HC-induced warming. Five out of six models used here include interactive tropospheric OH-CH_4 chemistry and therefore simulate changes in CH_4 lifetime associated with OH perturbations driven by ozone depletion. However, because CH_4 is prescribed as a lower boundary condition, part of the corresponding CH_4 concentration change is not included in the simulations. Previous studies estimate that ozone-induced CH_4 lifetime changes correspond to a radiative forcing of up to $-0.06\ W\ m^{-2}$[10,15]. This contribution is substantially smaller than the ozone SARF and the net ERF from OD-HCs. Its inclusion would modestly reduce the ERF values reported here; however, the net ERF remains positive, and our overall conclusions are unaffected. These conclusions differ from ref. 15 because we directly constrain the model ensemble with observed stratospheric ozone changes (JRA3Q, SWOOSH), rather than relying on the constrained value from ref. 8 based on total column ozone.

Uncertainties remain from potential nonlinear responses or rapid adjustments that are not fully captured by our regression framework[39], as well as methodological choices in deriving the ERF[40]. However, the spread across models–rather than being a limitation–provides the basis for applying observational constraints and deriving observation-based model weights. By leveraging the relationship between stratospheric ozone changes and OD-HC ERF, we establish a framework to handle physically implausible models and to obtain an observationally informed estimate for the climatic impacts of OD-HCs. Crucially, the strength of observational constraints ultimately depends on the availability and reliability of long-term ozone records. Although our findings very likely rule out a net cooling effect of OD-HCs, discrepancies among ozone datasets pose a significant source of uncertainty in the quantification of the OD-HC-induced ERF, underscoring

Table 1 | Number of ensemble members for simulations with transient forcings (columns 2 and 3) and number of years with top-of-atmosphere (TOA) radiative fluxes for time-slice simulations (columns 4 and 5)

Model	*historical*	*hist-1950HC*	*piClim-control*	*piClim-HC*
Name	(n# ens)	(n# ens)	(n# years)	(n# years)
CESM2-WACCM[51]	15	4	30	30
CNRM-ESM2-1[52]	11	3	30	30
GFDL-ESM4[53]	3	3	30	30
GISS-E2-1-G[54]	9	5	41	41
MRI-ESM2-0[55]	10	6	31	31
UKESM1-0-LL[56]	16	6	45	45
CESM1-WACCM[17,57]	6	6	–	–

the critical need to maintain and further improve ozone monitoring through satellite, ground-based networks, and reanalysis products.

Looking ahead, the interplay between the radiative effects of ozone and OD-HCs is expected to reverse: While historically ozone depletion has partially offset OD-HC-induced warming, future ozone recovery will contribute to global warming, while declining OD-HC concentrations will dampen it[40] have estimated that rising stratospheric ozone levels may produce warming exceeding the ODS-induced dampening (including OD-HCs), leading to a net positive contribution to future global warming[40]–in contrast to previous results[41–43]. Specifically,[40] found that ozone increases due to reduced OD-HC emissions between 2015 and 2050 lead to an ERF of $0.268 \pm 0.084\ W\ m^{-2}$, with roughly half attributable to OD-HC-induced changes, and an inferred radiative efficiency of ozone that is about three times larger than in IPCC AR6. A positive radiative forcing arising from ozone recovery of this magnitude would offset much of the negative radiative forcing projected from the phase-out of HCs, again raising questions about the net climate co-benefit of the Montreal Protocol[40]. Our results differ from those of[40] primarily because we focus on the historical period and diagnose emissionbased ERFs constrained by past observed ozone changes, rather than using future changes in ozone.

Most importantly, while the balance between future stratospheric ozone recovery and declining OD-HC concentrations remains uncertain, our findings give an independent and robust confirmation that halocarbons made a clear contribution to historical warming of about 20%, meaning that their phase-out under the Montreal Protocol has already averted a considerable amount of additional global warming. This statement is further supported by numerous "world-avoided" studies[6,34–38]. To further reduce remaining uncertainties, coordinated multi-model experiments and continued improvements in observational records are urgently required, particularly given the large inter-model spread in projected stratospheric ozone evolution[44] and the continued influence of greenhouse-gas driven climate change on the ozone layer[45].

Methods

Model experiments

The Aerosol Chemistry Model Intercomparison Project (AerChemMIP)[14] is a coordinated modeling initiative endorsed by the Coupled-Model Intercomparison Project 6 (CMIP6)[20]. It aims to quantify the climate and air quality impacts of near-term climate forcers (NTCFs) such as CH_4, tropospheric ozone, and aerosols, along with their precursors, nitrous oxide, and most importantly, ozone-depleting halocarbons (HCs). AerChemMIP seeks to quantify the contribution of anthropogenic emissions to global radiative forcing and surface climate until the year 2014. To tackle this question, AerChemMIP coordinated a set of model experiments using CMIP6 climate models that incorporate interactive tropospheric aerosols and atmospheric chemistry. First, a reference "historical" ensemble was driven with all observed anthropogenic and natural forcings compiled for CMIP6[20]. Then, a set of transient coupled-ocean simulations was designed, differing from the historical ensemble only in fixed anthropogenic emissions (or concentrations) of a specified class of chemical species. This framework isolates the climate impact of specific climate forcers, including OD-HCs, under realistic transient conditions.

We use output from all the chemistry-climate models participating in AerChemMIP that include interactive stratospheric chemistry. Compared to previous studies[7–9,21], our analysis incorporates additional ensemble members to improve statistical robustness, particularly ensemble members without increasing OD-HC abundances over the 20th century. We also included simulations with CESM1-WACCM from ref. 17. In total, four sets of experiments were used to estimate the impact of halocarbons on climate:

- *Transient historical coupled-ocean simulations (historical):* These simulations, that span the period 1850–2014, were forced with the historical emissions and atmospheric concentrations of different gases.
- *Transient historical fixed OD-HC simulations (hist-1950HC):* These simulations, analogous to the *historical* runs, but with OD-HC concentrations fixed at 1950 levels, cover the period 1950–2014, when OD-HC concentrations rose significantly.
- *Pre-industrial time-slice simulations (piClim-control):* In addition to the transient historical simulations, we analyse time-slice simulations using repeating boundary conditions for 1850. In these simulations, the same pre-industrial monthly varying SSTs and sea ice are prescribed (i.e., these are atmosphere-only AMIP-style experiments). In the control simulation *piClim-control* all the different climate forcers are fixed at their 1850 levels.
- *Pre-industrial time-slice historical with 2014 OD-HC concentrations (piClim-HC):* This set of simulations is identical to *piClim-control*, but imposing 2014 halocarbon concentrations to isolate the OD-HC-induced net ERF.

All experiments used in this study are summarized in Table 1.

Calculation of ERF and Ozone SARF

Here, we use *piClim-control* and *piClim-HC* experiments to quantify the ERF from historical OD-HC emissions, following the fixed sea surface temperature method (ERF_fSST) recommended by ref. 46, which has been utilized by refs. 7,8. For each model, the OD-HC ERF is calculated as the mean difference in the net top-of-atmosphere (TOA) radiative flux between *piClim-HC* and the *piClim-control* simulation, averaged over all available years of these time-slice experiments (between 30 and 45, Table 1). While sea surface temperatures (SSTs) are fixed, land-surface temperatures are allowed to adjust; however, this effect on the ERF is minimal[9] (their Fig. 3) and is thus neglected here. Uncertainty is estimated as the standard deviation of the yearly TOA radiative flux difference divided by the square root of the number of years per model. The ERF includes, by definition, the direct forcing due to the emission of OD-HCs, as well as the indirect forcing arising from changes in circulation, clouds, and, particularly, both stratospheric and indirect tropospheric chemical adjustments (e.g., changes in ozone, OH, and CH_4).

Stratospherically adjusted radiative forcing due to the OD-HC-induced ozone changes is estimated by radiative kernels from ref. 9, based on ref. 21. This approach excludes tropospheric adjustments, but can unambiguously isolate the stratospherically adjusted radiative forcing (SARF) arising from changes in atmospheric concentrations of certain species.

Observational datasets

To evaluate simulated ozone changes in AerChemMIP simulations and obtain observational constraints, we employ multiple observational and reanalysis products spanning different time periods. The JRA-55 reanalysis[47] from the Japan Meteorological Agency (JMA) provides data from 1958 onward, in a horizontal resolution of 2.5°, with 37 vertical levels

up to 1 hPa. After 1978, stratospheric ozone is assimilated from observations in this product, while prior to that period, a climatological monthly mean ozone field, derived over 1980–1984, is used. Therefore, no reliable estimates for stratospheric ozone changes before 1978 can be derived from this product. JRA-3Q[23,24] from JMA extends to 1947 with a horizontal resolution of TL479 and 100 vertical levels up to 0.01 hPa. Similar to JRA-55, it assimilates ozone after 1979. Before that, ozone fields are calculated using the fully coupled chemistry-climate model MRI-CCM2.1 with nudged winds derived from JRA-55, and this ozone is subsequently bias-corrected and used as forcing in the reanalysis product. Ozone before 1978 is therefore not fully observational-based, while being based on assimilated wind fields. JRA-3Q generally offers notable improvements in the stratosphere compared to JRA-55, especially in the QBO, despite some underestimations of the cooling following major volcanic eruptions.

The satellite-based "Stratospheric Water and Ozone Satellite Homogenized" (SWOOSHv2.6)[33] provides a fully observational-based dataset of zonal-mean monthly-mean ozone mixing ratios, by merging and homogenizing multiple ozone satellite records into a consistent time series. Lastly, NIWA-BS (version 3.4.1)[48] provides observational and homogenized total column ozone records from 1978 onward, being derived from multiple satellite instruments, with additional corrections from ground-based measurements.

Moreover, the CMIP6 ozone forcing dataset[19] is compared against observations and reanalysis as well as AerChemMIP simulations. This dataset is provided through the input data sets for Model Intercomparison Projects (input4MIPs) and used in CMIP6 models without interactive ozone chemistry, including models that have previously been used to assess the climatic impacts of OD-HCs[18]. The new CMIP7 forcing data set is very similar and gives similar results.

Calculation of partial and total ozone column

We calculate the stratospheric partial column ozone (PCO) and total column ozone (TCO) columns as follows:

$$O_{3,pcol} = \frac{1DU}{2.687 \cdot 10^{16}\ \frac{molec}{cm^2}} \sum_{p=lower\_p}^{upper\_p} \frac{\chi_{O_3}(p) \cdot 10 \cdot \Delta p}{g \cdot m_{air,d}} \quad (1)$$

with $\chi_{O_3}(p)$ being ozone mixing ratio at pressure level p, Δp the thickness of the respective pressure level, g is the gravitational constant (in $\frac{cm}{s^2}$) and $m_{air,d}$ the mass of dry air (in $\frac{g}{molec}$)[49]. For stratospheric PCO, we set *lower_p* to 100 hPa and *upper_p* to 30 hPa, whereas we use, the boundaries 1000 hPa (*lower_p*) and 0.01 hPa (*upper_p*) for TCO.

Observational constraints

Given the strong linear correlation between the OD-HC ERF and historical ozone changes, with the latter being an observable quantity, we apply observational constraints to reduce the uncertainty in the ERF estimates[50]. In total, we use one observational dataset (JRA-3Q) for the historical period (1955–2005) and three observational datasets (JRA-3Q, JRA-55, SWOOSH) for the satellite period (1985–2005) to derive four individual estimates for the OD-HC ERF. The "best guess" (ERF_{bg}) is obtained via linear regression between modeled ozone changes and ERF, and then evaluating this regression at the observed PCO change ΔPCO_{obs}:

$$ERF_{bg} = s_1 \cdot \Delta PCO_{obs} + y_1, \quad (2)$$

where s_1 and y_1 denote the slope and intercept of the regression, respectively. The uncertainty in the estimate is therefore dependent on uncertainties in the observed PCO change, as well as uncertainties in the slope and intercept of the regression. The latter in turn depends on the uncertainties in the modeled ozone change and the models' ERF estimate–and therefore on internal variability in models. To estimate the overall resulting uncertainty of the "best guess" ERF (resulting from interannual variability in model simulations and observations, differences across ensemble members, and regression uncertainty), we use the following re-sampling procedure, allowing us to derive a probability density function for the ERF:

- For each climate model, we perform bootstrap resampling of partial ozone column changes from the available ensemble members. Each resampling step is conducted with replacement, and the bootstrap sample size is equal to the number of ensemble members for a given model. For each model, the mean across all bootstrap samples is then calculated, providing one value for each model.
- For each model, we draw one OD-HC ERF value from a normal distribution defined by the mean and standard deviation obtained from the corresponding pairs of piClim experiments. This step captures the model-specific uncertainty in the ERF of OD-HCs.
- We pair the ERF values from steps (1) and (2) across the six models, and perform ordinary least squares linear regression to estimate the slope and intercept of the emergent relationship. The intercept reflects the direct ERF of OD-HCs in the absence of ozone depletion.
- From the observational datasets, we sample a single value of the partial ozone column change from a normal distribution defined by its observed mean and standard deviation.
- The constrained ERF of OD-HCs is obtained by using the regression parameters (slope and intercept) together with the sampled value of the observational dataset.
- The previous steps are performed 10^6 times, resulting in a distribution of one million OD-HC net ERF estimates and one million intercept values.

To constrain the contribution of OD-HCs to past global temperature change, we calculate weighted multi-model means with weights based on the level of agreement between simulated and observed stratospheric ozone changes. In addition to the six models that participated in AerChemMIP[14], we include CESM1-WACCM from ref. 17 (in Fig. 4b, c). We derive both weighted multi-model means for the absolute and relative contributions of OD-HCs to 1955–2005 global warming with weighting based on either SWOOSH (1985–2005) or JRA-3Q (1955–2005) ozone changes. In the model weighting scheme described in the following, we propagate uncertainty in (i) observations or reanalysis, (ii) the simulated changes in stratospheric ozone, and (iii) the simulated changes in surface temperature.

For the seven models, we consider global and ensemble mean values of PCO changes in the historical period and the satellite period (for comparison with JRA-3Q and SWOOSH, respectively); however, for the satellite period, we again exclude GISS-E2-1-G. The uncertainty in modeled ozone changes is given by the standard error of the mean (i.e., the standard deviation across the ensemble divided by the square root of the ensemble size). For JRA-3Q and SWOOSH, we consider both their mean change (μ_{obs}) and standard deviation in the change (σ_{obs}). We perform 10^6 iterations of the following Monte Carlo sampling:

- For each model, we draw one value for the PCO change from a normal distribution centered on the model's ensemble mean and standard deviation given by its standard error. This yields a set of seven model values (M).
- We draw a single observation-derived value from a normal distribution with mean μ_{obs} and standard deviation σ_{obs}.
- We normalize both the model-simulated and observation-derived ozone values to the [0, 1] range using the minimum and maximum of the model ensemble (min(M) and max(M), respectively) for consistent scaling.
- We calculate model weights according to a Gaussian kernel:

$$w_i = \exp\left[-\frac{(m_i - o)^2}{2\sigma_w^2}\right] \quad (3)$$

Here, m_i and o denote the normalized model and observed changes in PCO, respectively. $\sigma_w = \sigma_{\text{obs}}/(\max(M) - \min(M))$ defines the the width of the weighting kernel. The weights are subsequently normalized such that $\sum_i w_i = 1$.

- At the same time, we take bootstrap samples of the global mean surface temperature change for each model's *historical* and *hist-1950HC* ensemble and average them. We thereby obtain one estimate per iteration and model for the historical surface temperature change ($\Delta T_{hist,i}$) and the OD-HC-induced surface temperature change ($\Delta T_{HC,i} = \Delta T_{hist,i} - \Delta T_{1950HC,i}$).
- We then calculate weighted ensemble means as

$$\overline{\Delta T}_{HC} = \sum_i w_i \cdot \Delta T_{\text{HC,i}}, \ \overline{\Delta T}_{hist} = \sum_i w_i \cdot \Delta T_{hist,i}. \quad (4)$$

- Finally, we calculate the weighted fractional contribution of OD-HCs to surface warming (f_{tas}^{HC}) by the following ratio:

$$f_{tas}^{HC} = \sum_i w_i \cdot \frac{\Delta T_{HC,i}}{\Delta T_{hist,i}} \quad (5)$$

In the end, this yields empirical distributions of the OD-HC-induced absolute and relative contribution to surface temperature change over the second half of the 20th century (1955–2005).

Data availability

AerChemMIP data can be downloaded from the Earth System Grid Federation (ESGF) server: https://aims2.llnl.gov/search/cmip6/. Additional ensemble members simulated for this study, as well as the WACCM4 data from[17], will be made available upon request. JRA-3Q and JRA-55 data can be downloaded from the National Center for Atmospheric Research (NCAR) homepage: https://gdex.ucar.edu/datasets/d640000/and https://gdex.ucar.edu/datasets/d628001/. SWOOSH ozone data can be downloaded from the National Oceanic and Atmospheric Administration (NOAA) homepage: https://www.ncei.noaa.gov/access/metadata/landing-page/bin/iso?id=gov.noaa.ncdc:C00958. Finally, NIWA-BS total ozone column data is available on Zenodo: https://zenodo.org/records/4535293.

Code availability

The code used for data analysis alongside some intermediary data files can be found here: https://doi.org/10.5281/zenodo.19465624.

Received: 15 December 2025; Accepted: 20 March 2026;
Published online: 30 April 2026

References

1. Solomon, S. Stratospheric ozone depletion: a review of concepts and history. *Rev. Geophys.* **37**, 275–316 (1999).
2. World Meteorological Organization (WMO). Executive summary. scientific assessment of ozone depletion: 2022. Technical Report 278 (World Meteorological Organization (WMO), 2022).
3. Wigley, T. M. L. Future CFC concentrations under the Montreal Protocol and their greenhouse-effect implications. *Nature* **335**, 333–335 (1988).
4. Hodnebrog, Ø et al. Global warming potentials and radiative efficiencies of halocarbons and related compounds: a comprehensive review. *Rev. Geophys.* **51**, 300–378 (2013).
5. Hodnebrog, Ø. et al. Updated global warming potentials and radiative efficiencies of halocarbons and other weak atmospheric absorbers. *Rev. Geophys.* **58**, https://agupubs.onlinelibrary.wiley.com/doi/abs/10.1029/2019RG000691 (2020).
6. Velders, G. J. M., Andersen, S. O., Daniel, J. S., Fahey, D. W. & McFarland, M. The importance of the Montreal Protocol in protecting climate. *Proc. Natl. Acad. Sci.* **104**, 4814–4819 (2007).
7. Morgenstern, O. et al. Reappraisal of the climate impacts of ozone-depleting substances. *Geophys. Res. Lett*. **47**, https://doi.org/10.1029/2020GL088295 (2020).
8. Morgenstern, O., Frith, S. M., Bodeker, G. E., Fioletov, V. & A, R. J.Reevaluation of total column ozone trends and of the effective radiative forcing of ozone-depleting substances. *Geophys. Res. Lett.* **48**, https://doi.org/10.1029/2021GL095376 (2021).
9. Thornhill, G. D. et al. Effective radiative forcing from emissions of reactive gases and aerosols a multi-model comparison. *Atmos. Chem. Phys.* **21**, 853–874 (2021).
10. Szopa, S. et al. Short-lived climate forcers supplementary material. in *Climate Change 2021: the Physical Science Basis. Contribution of Working Group I to the Sixth Assessment Report of the Intergovernmental Panel on Climate Change*, (eds. Masson-Delmotte, V. et al.) book section 6,1–24. https://www.ipcc.ch/report/ar6/wg1/downloads/report/IPCC_AR6_WGI_Chapter06_SM.pdf (Cambridge University Press, 2021).
11. Forster, P. et al. The Earth's energy budget, climate feedbacks, and climate sensitivity. in *Climate Change 2021: the Physical Science Basis. Contribution of Working Group I to the Sixth Assessment Report of the Intergovernmental Panel on Climate Change*, (eds. Masson-Delmotte, V. et al.) book section 7, 923–1054. https://www.ipcc.ch/report/ar6/wg1/downloads/report/IPCC_AR6_WGI_Chapter07.pdf (Cambridge University Press,Cambridge, 2021).
12. Solomon, S. & Daniel, J. S.Impact of the Montreal Protocol and its amendments on the rate of change of global radiative forcing. *Clim. Change* **32**, 7–17 (1996).
13. Ramaswamy, V., Schwarzkopf, M. & Shine, K. Radiative forcing of climate from halocarbon-induced global stratospheric ozone loss. *Nature* **355**, 810–812 (1992).
14. Collins, W. J. et al. AerChemMIP: quantifying the effects of chemistry and aerosols in CMIP6. *Geosci. Model Dev.* **10**, 585–607 (2017).
15. Collins, W. J. et al. Indirect climate forcing from ozone depleting substances. *EGUsphere* **2026**, 1–28 (2026).
16. Sherwood, S. C. et al. An assessment of Earth's climate sensitivity using multiple lines of evidence. *Rev. Geophys.* **58**, e2019RG000678 (2020).
17. Polvani, L. M., Previdi, M., England, M. R., Chiodo, G. & Smith, K. L. Substantial twentieth-century arctic warming caused by ozone-depleting substances. *Nat. Clim. Change* **10**, 130–133 (2020).
18. Sigmond, M. et al. Large contribution of ozone-depleting substances to global and arctic warming in the late 20th century. *Geophys. Res. Lett.* **50**, e2022GL100563 (2023).
19. Checa-Garcia, R., Hegglin, M. I., Kinnison, D., Plummer, D. A. & Shine, K. P. Historical tropospheric and stratospheric ozone radiative forcing using the CMIP6 database. *Geophys. Res. Lett.* **45**, 3264–3273 (2018).
20. Eyring, V. et al. Overview of the coupled model intercomparison project phase 6 (CMIP6) experimental design and organization. *Geosci. Model Dev.* **9**, 1937–1958 (2016).
21. Skeie, R. B., Myhre, G., Hodnebrog, Ø. et al. Historical total ozone radiative forcing derived from CMIP6 simulations. *npj Clim. Atmos. Sci.* **3**, https://doi.org/10.1038/s41612-020-00131-0 (2020).
22. Forster, P. et al. The Earth's energy budget, climate feedbacks, and climate sensitivity supplementary material. in *Climate Change 2021: the Physical Science Basis. Contribution of Working Group I to the Sixth Assessment Report of the Intergovernmental Panel on Climate Change* (eds. Masson-Delmotte, V. et al.), book section 7,1–35. https://www.ipcc.ch/report/ar6/wg1/downloads/report/IPCC_AR6_WGI_Chapter07_SM.pdf (Cambridge University Press, 2021)

23. Naoe, H., Kobayashi, C., Kobayashi, S., Kosaka, Y. & Shibata, K. Representation of quasi-biennial oscillation in JRA-3q. *J. Meteorol. Soc. Jpn. Ser. II* **103**, 233–255 (2025).
24. Kosaka, Y. et al. The JRA-3Q Reanalysis. *J. Meteorol. Soc. Jpn. Ser. II* **102**, 49–109 (2024).
25. Shindell, D. et al. Attribution of historical ozone forcing to anthropogenic emissions. *Nat. Clim. Change* **3**, 567–570 (2013).
26. Randel, W. J. et al. An update of observed stratospheric temperature trends. *J. Geophys. Res. Atmos.* **114**, https://agupubs.onlinelibrary.wiley.com/doi/abs/10.1029/2008JD010421 (2009).
27. Chiodo, G. & Polvani, L. M. New insights on the radiative impacts of ozone-depleting substances. *Geophys. Res. Lett.* **49**, e2021GL096783 (2022).
28. Santer, B. D. et al. Contributions of anthropogenic and natural forcing to recent tropopause height changes. *science* **301**, 479–483 (2003).
29. Aquila, V. et al. Isolating the roles of different forcing agents in global stratospheric temperature changes using model integrations with incrementally added single forcings. *J. Geophys. Res. Atmos.***121**, 8067–8082 (2016).
30. Szopa, S. et al. Short-lived climate forcers. in *Climate Change 2021: the Physical Science Basis. Contribution of Working Group I to the Sixth Assessment Report of the Intergovernmental Panel on Climate Change* (eds. Masson-Delmotte, V. et al.) book section 6, 817–921. https://www.ipcc.ch/report/ar6/wg1/downloads/report/IPCC_AR6_WGI_Chapter06.pdf. (Cambridge University Press, 2021).
31. O'Connor, F. M. et al.Assessment of pre-industrial to present-day anthropogenic climate forcing in UKESM1. *Atmos. Chem. Phys.***21**, 1211–1243 (2021).
32. Forster, P., Ramaswamy, V., Artaxo, P., Berntser, T. & Betts, R. Changes in atmospheric constituents and in radiative forcing. *Climate Change 2007: the Physical Science Basis. Contribution of Working Group I to the Fourth Assessment Report of the Intergovernmental Panel on Climate Change* (eds. Solomon, S. et al.), book section 2, 129–234. https://archive.ipcc.ch/report/ar4/wg1/ (Cambridge University Press, 2021).
33. Davis, S. M. et al. The Stratospheric Water and Ozone Satellite Homogenized (SWOOSH) database: a long-term database for climate studies. *Earth Syst. Sci. Data* **8**, 461–490 (2016).
34. Garcia, R. R., Kinnison, D. E. & Marsh, D. R. "World avoided" simulations with the whole atmosphere community climate model. *J. Geophys. Res. Atmos.* **117**, https://agupubs.onlinelibrary.wiley.com/doi/abs/10.1029/2012JD018430 (2012).
35. Egorova, T., Rozanov, E., Gröbner, J., Hauser, M. & Schmutz, W. Montreal protocol benefits simulated with CCM Socol. *Atmos. Chem. Phys.* **13**, 3811–3823 (2013).
36. Goyal, R., England, M. H., Sen Gupta, A. & Jucker, M. Reduction in surface climate change achieved by the 1987 Montreal Protocol. *Environ. Res. Lett.* **14**, 124041 (2019).
37. Zilker, F. et al. Stratospherically induced circulation changes under the extreme conditions of the no-Montreal-Protocol scenario. *Atmos. Chem. Phys.* **23**, 13387–13411 (2023).
38. England, M. R. & Polvani, L. M. The Montreal Protocol is delaying the occurrence of the first ice-free Arctic summer. *Proc. Natl. Acad. Sci.* **120**, e2211432120 (2023).
39. Ramaswamy, V. et al. Radiative forcing of climate: The historical evolution of the radiative forcing concept, the forcing agents and their quantification, and applications. *Meteorol. Monogr.* **59**, 14–1 (2019).
40. Collins, W. J. et al. Climate forcing due to future ozone changes: an intercomparison of metrics and methods. *Atmos. Chem. Phys.* **25**, 9031–9060 (2025).
41. Bekki, S. et al. Climate impact of stratospheric ozone recovery. *Geophys. Res. Lett.* **40**, 2796–2800 (2013).
42. Iglesias-Suarez, F. et al. Key drivers of ozone change and its radiative forcing over the 21st century. *Atmos. Chem. Phys.* **18**, 6121–6139 (2018).
43. Banerjee, A., Maycock, A. C. & Pyle, J. A. Chemical and climatic drivers of radiative forcing due to changes in stratospheric and tropospheric ozone over the 21st century. *Atmos. Chem. Phys.* **18**, 2899–2911 (2018).
44. Chiodo, G. et al. The influence of future changes in springtime arctic ozone on stratospheric and surface climate. *Atmos. Chem. Phys.* **23**, 10451–10472 (2023).
45. Keeble, J. et al. Evaluating stratospheric ozone and water vapour changes in CMIP6 models from 1850 to 2100. *Atmos. Chem. Phys.* **21**, 5015–5061 (2021).
46. Forster, P. M. et al. Recommendations for diagnosing effective radiative forcing from climate models for CMIP6: Recommended Effective Radiative Forcing. *J. Geophys. Res. Atmos.* **121**, 12,460–12,475 (2016).
47. Ebita, A. et al. The japanese 55-year reanalysis: an interim report. *SOLA* **7**, 149–152 (2011).
48. Bodeker, G. E. et al. Niwa-bs total column ozone database v3.4.1. https://doi.org/10.5281/zenodo.7447660 (2023)
49. Friedel, M., Chiodo, G. & Stenke, A. Springtime Arctic ozone depletion forces northern hemisphere climate anomalies. *Nat. Geosci.* **15**, 541–547 (2022).
50. Simpson, I. R. et al. Emergent constraints on the large-scale atmospheric circulation and regional hydroclimate: Do they still work in CMIP6 and how much can they actually constrain the future?. *J. Clim.* **34**, 6355 – 6377 (2021).
51. Gettelman, A. et al. The whole atmosphere community climate model version 6 (WACCM6). *J. Geophys. Res. Atmos.* **124**, 12380–12403 (2019).
52. Séférian, R. et al. Evaluation of CNRM Earth System Model, CNRMESM21: role of earth system processes in present-day and future climate. *J. Adv. Model. Earth Syst.* **11**, 4182–4227 (2019).
53. Dunne, J. P. et al. The GFDL Earth System Model version 4.1 (GFDLESM 4.1): overall coupled model description and simulation characteristics. *J. Adv. Mod. Earth Syst.* **12** https://doi.org/10.1029/2019MS002015 (2020).
54. Kelley, M. et al. GISSe2.1: configurations and climatology. *J. Adv. Mod. Earth Syst.* **12**, https://doi.org/10.1029/2019MS002025 (2020).
55. Yukimoto, S. et al. The Meteorological Research Institute Earth System Model version 2.0, MRI-ESM2.0: description and basic evaluation of the physical component. *J. Meteorol. Soc. Jpn. Ser.* II **97**, 931–965 (2019).
56. Sellar, A. A. et al. UKESM1: description and evaluation of the UK Earth System Model. *J. Adv. Model. Earth Syst*. **11**, 4513–4558 (2019).
57. Marsh, D. R. et al. Climate change from 1850 to 2005 simulated in CESM1 (WACCM). *J. Clim.* **26**, 7372–7391 (2013).

Acknowledgements

N.L.A. and J.K. used Monsoon2, a collaborative High-Performance Computing facility funded by the Met Office and the Natural Environment Research Council. We thank Urs Beyerle (IAC ETH) for support in acquiring and post-processing the AerChemMIP data. N.O. was supported by the Environment Research and Technology Development Fund (JPMEERF20232001) of the Environmental Restoration and Conservation Agency provided by Ministry of the Environment of Japan, the Arctic Challenge for Sustainability 3 (ArCS-3), Program Grant Number JPMXD1720251001, and a grant for the Global Environmental Research Coordination System from Ministry of the Environment of Japan (MLIT2253). G.C. was supported by the European Union via the ERC Starting Grant - number 101078127. Supported by the Open Access Publishing Fund of Leipzig University

Author contributions

G.C., M.F., and K.W. conceived the study. N.L.A., M.D., N.O., L.W.O., J.F., J.K., L.N., and C.O. conducted the modeling experiments. M.F. and K.W. analyzed and interpreted the results with extensive input from G.C. M.F. wrote the paper, with input from G.C., K.W, J.S.D., and L.M.P. G.C., M.F., K.W., J.D., L.P., J.S.D., N.L.A., S.M.D., M.D., N.O., L.W.H., J.F.L., J.K., L.N., and C.O. discussed the results and contributed to the final manuscript. We confirm that all authors have read and approved the manuscript.

Funding
Open Access funding enabled and organized by Projekt DEAL.

Competing interests
The authors declare no competing interests.

Additional information
Supplementary information The online version contains supplementary material available at https://doi.org/10.1038/s41612-026-01398-5.

Correspondence and requests for materials should be addressed to M. Friedel, G. Chiodo or K. Weber.

Reprints and permissions information is available at http://www.nature.com/reprints

Publisher's note Springer Nature remains neutral with regard to jurisdictional claims in published maps and institutional affiliations.

Open Access This article is licensed under a Creative Commons Attribution 4.0 International License, which permits use, sharing, adaptation, distribution and reproduction in any medium or format, as long as you give appropriate credit to the original author(s) and the source, provide a link to the Creative Commons licence, and indicate if changes were made. The images or other third party material in this article are included in the article's Creative Commons licence, unless indicated otherwise in a credit line to the material. If material is not included in the article's Creative Commons licence and your intended use is not permitted by statutory regulation or exceeds the permitted use, you will need to obtain permission directly from the copyright holder. To view a copy of this licence, visit http://creativecommons.org/licenses/by/4.0/.

© The Author(s) 2026